

Voltammetry Behavior of Modified Carbon Paste Electrode with Cytochrome C and Mn₂O₃ Nanoparticles for Hydrogen Peroxide Sensing

Gholamreza Mohseni¹, Masoud Negahdary^{2,*}, Hossein Faramarzi³, Shokoufeh Mehrtashfar⁴, Amir Habibi-Tamijani⁵, Seyyed Hossein Nazemi⁶, Zeinab Morshedtalab⁷, Manouchehr Mazdapour⁸ and Sara Parsania⁷

¹ Department of Anesthetics, Shahid Beheshti University of Medical Sciences, Tehran, Iran

² Young Researchers & Elite Club, Marvdasht Branch, Islamic Azad University, Marvdasht, Iran

³ Infectious Disease Specialist, Department of Social Medicine, Shiraz University of Medical Sciences, Shiraz, Iran

⁴ Department of Biology, Guilan University, Guilan, Iran

⁵ Department of Chemistry, Mashhad Branch, Islamic Azad University, Mashhad, Iran

⁶ Department of Operating and Anesthesia, School of Paramedicine, Gonabad University of Medical Sciences, Gonabad, Iran

⁷ Department of Biology, Payame Noor University, I.R. of IRAN

⁸ Department of Biology, Islamic Azad University, pharmaceutical science Branch, Tehran, Iran

*E-mail: masoud.negahdary@hotmail.com

Received: 8 September 2012 / Accepted: 22 October 2012 / Published: 1 December 2012

In this research, we studied voltammetry behavior of modified carbon paste electrode (CPE) with Cytochrome C (Cyt_c) and Manganese oxide (Mn₂O₃) nanoparticles (Nps) for hydrogen peroxide (H₂O₂) sensing. Mn₂O₃ nanoparticles was synthesized from Mn (III) acetylacetonate; and Synthesized Mn₂O₃ Nps was characterized by XRD (X-ray diffraction), UV-visible (), SEM (scanning electron microscopy) and TEM (transmission electron microscopy) analysis. The average diameter of the Synthesized Mn₂O₃ Nps estimated about 70 nanometer (nm). Cyclic voltammetry (CV) was used to characterize the modification of electrodes in the potential range of -200 – -600 mV in 0.1M PBS (pH 7.0); the CVs of Cyt_c / Mn₂O₃ Nps / CPE give a pair of well-defined redox peaks at -500 and -475 mV at scan rate of 100 mV/s⁻¹ respectively and also in this measurement, ΔE = 25 mV and formal potential (E⁰) = -487.5. Cyt_c structure could change oxidative iron state (Fe³⁺) to reductive state (Fe²⁺) and vice versa by electron transfer. We used of this electron transfer in designing a new biosensor for H₂O₂ detection and designed biosensor could detect H₂O₂ in range of 15 to 225 μM.

Keywords: Bioelectrochemistry, Cytochrome C, Mn₂O₃ nanoparticles, hydrogen peroxide

1. INTRODUCTION

Nanotechnology is concerned with materials and systems whose structures and components exhibit novel and significantly improved physical, chemical, and biological properties, phenomena, and processes due to their nanoscale size [1-3]. The goal is to exploit these properties by gaining control of structures and devices at atomic, molecular and supramolecular levels and to learn to efficiently manufacture and use these devices [4-5]. Nps that is, particles with core diameters of 1-100 nm possessing unique chemical and physical properties arising from their nanoscale dimensions continue to be of significant current interest for their potential applications in catalysis, quantum computers, optical, electronic, or magnetic devices, chemical sensors, ferrofluids for cell separations, as components in industrial lithography or in photochemical devices such as flat-panel displays [6-9]. In each of these applications the size and size distribution of the nanoparticles are a primary concern [10]. In this research work, we investigated voltammetry behavior of modified CPE with Cyt_c and Mn₂O₃ Nps for H₂O₂ sensing. Voltammetry is the general name given to a group of electroanalytical methods in which the current is measured as a function of applied potential wherein the polarization of the indicator or working electrode is enhanced [11-14]. The measurement of a current is done when the complete concentration polarization takes place in an electrochemical cell. CV is an attractive voltammetric method for the learning of basic concepts in electrochemistry [15-16]. In brief, it is perhaps the most versatile electrochemical technique for the study of electroactive species. The effectiveness of CV results from its capability for rapidly observing the redox behavior over a wide range of potential [17]. Cyt_c is an ancient protein, developed early in the evolution of life. Since this essential protein performs a key step in the production of cellular energy, it has changed little in millions of years [18-20]. So, you can look into yeast cells or plant cells or our own cells and find a very similar form of Cyt_c. This protein is a carrier of electrons [21-22]. Like many proteins that carry electrons, it contains a special prosthetic group that handles the slippery electrons. Cyt_c contains a heme group with an iron ion gripped tightly inside. The iron ion readily accepts and releases an electron [23]. The Fe (III)/Fe (II) redox state could be found in Cyt_c by electron exchange [24-25]. The Three-dimensional structure of Cyt_c was shown in figure 1 [18-20].

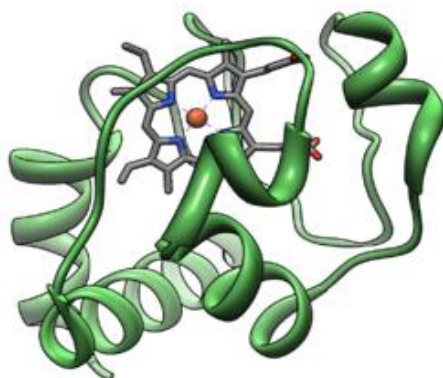


Figure 1. Three-dimensional structure of Cyt_c.

Biosensors are generally developed for the detection of analytes in the liquid phase, particularly in aqueous phase that is close to the physiological environment of the biomolecules used [26-29]. The strength of biosensors is their high selectivity due to the specific interaction between the biomolecule receptor and the analyte [30]. For example in this work our analyte was H_2O_2 . The determination of H_2O_2 is of considerable interest, because hydrogen peroxide is not only an important analyte in food, pharmaceutical, clinical, industrial and environmental analyses but also playing a key role as the product of the enzymatic reaction in coupled enzyme systems [31-33]. Several analytical techniques have been employed for this determination, such as titrimetry [34], spectrometry [35], Chemiluminescence [36], but these techniques suffer from interferences, long analysis time and use of expensive reagents. Electroanalytical methods [37] have also been found suitable since they achieve low detection limits and rapid response time. Here we used of Nanoscience, biology and electrochemical method for designing a new biosensor for H_2O_2 detection.

2. EXPERIMENTAL

2.1. Materials

Cyt_c and Mn (III) acetylacetonate purchased from Sigma-Aldrich. Other Reagents such as H_2O_2 purchased from Merck. The supporting electrolyte used for all experiments was 0.1 M pH 7 phosphate buffer solution (PBS), which prepared by using 0.1 M Na_2HPO_4 and NaH_2PO_4 solutions. All the reagents used were of analytical grade and all aqueous solutions were prepared using doubly distilled water generated by a Barnstead water system.

2.2. Apparatus

CV were performed using an Autolab potentiostat PGSTAT 302 (Eco Chemie, Utrecht, The Netherlands) driven by the General purpose Electrochemical systems data processing software (GPES, software version 4.9, Eco Chemie). A conventional three-electrode cell was employed throughout the experiments, with bare or Mn_2O_3 Nps modified CPE (3.0mm diameter) as a working electrode, a saturated calomel electrode (SCE) as a reference electrode, and a platinum electrode as a counter electrode; Reference and counter electrodes were purchased from Azar electrode Co (IR. Iran). The phase characterization of Mn_2O_3 Nps was performed by means of XRD using a D/Max-RA diffractometer with $\text{CuK}\alpha$ radiation. The absorbance properties of prepared nanoparticles were measured and recorded by using a TU-1901 double-beam UV-visible spectrophotometer. The morphologies and particle sizes of the samples were characterized by JEM-200CX TEM working at 200 kV, and SEM image was obtained with a ZIESS EM 902A SEM.

2.3. Preparation of Mn_2O_3 Nps

Mn_2O_3 Nps were synthesized by heating Mn (III) acetylacetonate (1 mmol, 0.35 g) in 20 mL acetone or ethanol in a Teflon-lined Parr acid-digestion bomb at 200°C for a minimum of 72 hours.

The dark product solution was dispersed in chloroform and centrifuged for 10 minutes. The black precipitate was isolated and dried at Room Temperature under vacuum for 12 hours, followed by calcination at 500°C for 4 hours. The product was characterized by XRD, UV-visible, SEM and TEM analysis.

2.4. Preparation of unmodified CPE and modified CPE with Mn_2O_3 Nps

Unmodified CPE was prepared by mixing 65% graphite powder and 35% paraffin wax. Paraffin wax was heated till melting and then, mixed very well with graphite powder to produce a homogeneous paste. The resulted paste was then packed into the end of an insulin syringe (i.d.: 3.0mm). External electrical contact was established by forcing a copper wire down the syringe. CPE modified with Mn_2O_3 Nanoparticles was prepared by mixing 60% graphite powder and 30% paraffin wax with and 10% Mn_2O_3 Nps. The surface of the electrode was polished with a piece of weighting paper and then rinsed with distilled water thoroughly.

2.5. Preparation of Cyt_c - Mn_2O_3 Nps modified CPE

The modified CPE electrode that produced in previous section was used for production of Cyt_c - Mn_2O_3 Nps modified CPE. In this section, the Cyt_c was immobilized by dropping 3 μ l of 10 mg/ml of the protein solution onto the Mn_2O_3 Nps modified CPE and dried for about 30 min at room temperature. The electrode was then gently washed with de-ionized double distilled water and put at 4 °C when not in use.

3. RESULTS AND DISCUSSION

3.1. UV-visible spectroscopy of Mn_2O_3 Nps

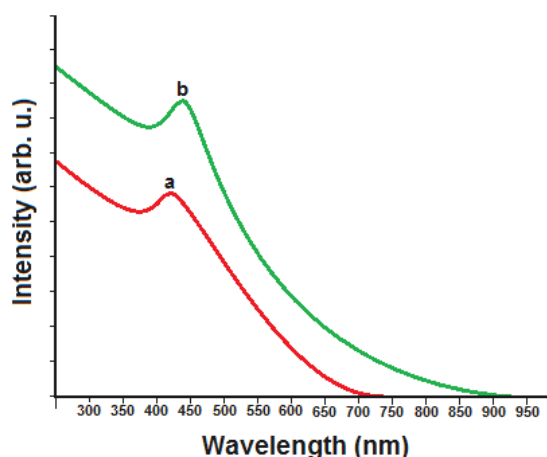


Figure 2. UV-visible spectroscopy for (a) bulk Mn_2O_3 particles; (b) Mn_2O_3 Nps.

UV-visible spectroscopy is one of the most widely used techniques for structural characterization of metal nanoparticles [38]. These nanoparticles exhibit a strong UV-vis absorption band that is not present in the spectrum of the bulk state [39]. The UV-VIS spectral range is approximately 190 to 900 nm, as defined by the working range of typical commercial UV-VIS spectrophotometers. According to Fig. 2(a&b), you can see that in nano size state, material show a different UV-VIS spectra ratio to bulk state. As it is clear, intensity units was increased and improved in Mn_2O_3 Nps (Fig. 2(b)) due to the quantum confinement of the excitons present in the sample compare with bulk Mn_2O_3 particles (Fig. 2(a)). This phenomenon indicates that these Nps show the quantum size effect [40].

3.2. X-Ray diffraction of Mn_2O_3 Nps

The XRD pattern Fig. 3 for Mn_2O_3 Nps, the diffraction peaks are absorbed at 2θ values. The prominent peaks have been utilized to estimate the grain size of sample with the help of Scherrer equation [41] $D = K\lambda/(\beta \cos \theta)$ where K is constant(0.9), λ is the wavelength($\lambda = 1.5418 \text{ \AA}$) (Cu $K\alpha$), β is the full width at the half-maximum of the line and θ is the diffraction angle. The grain size estimated using the relative intensity peak for Mn_2O_3 Nps was found to be 70 nm and increase in sharpness of XRD peaks indicates that particles are in crystalline nature. All peaks in Fig. 3 related to Mn_2O_3 Nps and matched to Joint Committee for Powder Diffraction Studies (JCPDS).

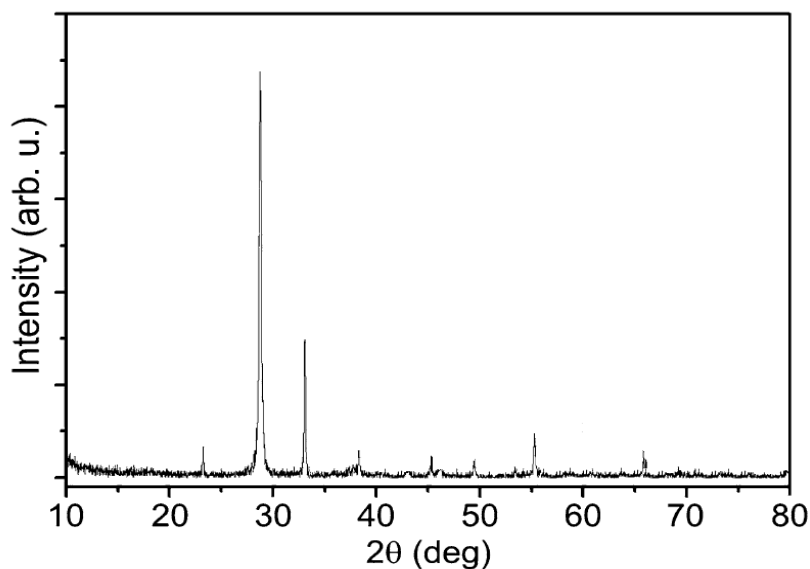


Figure 3. XRD pattern for Mn_2O_3 Nps.

3.3. Microscopic characterization of Mn_2O_3 Nps

As it is well known, the properties of a broad range of materials and the performance of a large variety of devices depend strongly on their surface characteristics. Morphology of the Mn_2O_3 Nps was investigated by using of TEM and SEM. Parts (a) and (b) of Fig. 4 show the typical TEM and SEM

images of the sample respectively. The SEM image was captured in 1 μm scale bar and the TEM image was captured in 100 nm scale bar. The average diameter of the Synthesized Mn_2O_3 Nps was about 70 nm, and had a very narrow particle distribution.

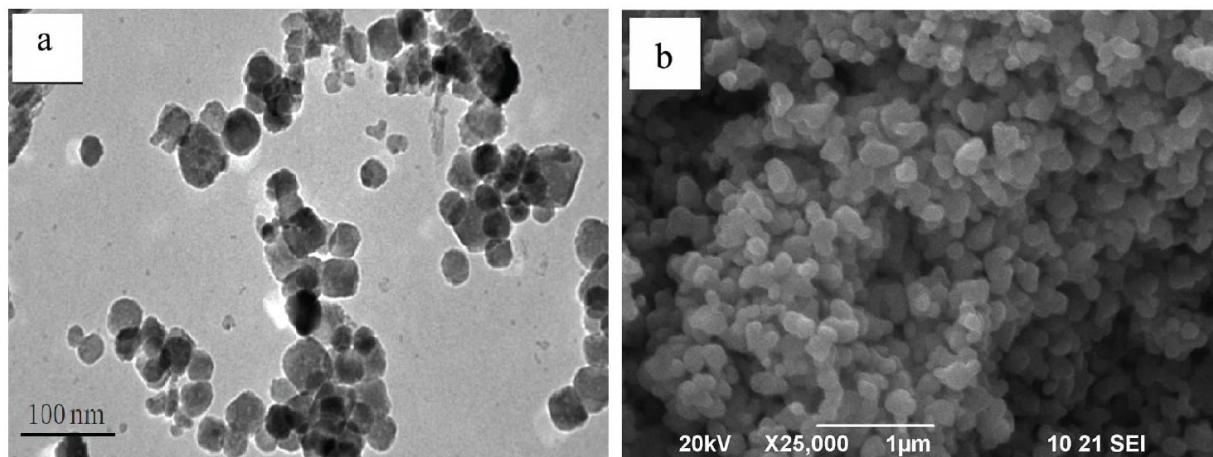


Figure 4. (a) TEM image and (b) SEM image, of Mn_2O_3 NPs.

3.4. Direct electrochemistry of the modified CPE with Cyt_c and Mn_2O_3 Nps

CV was used to characterize the modification of electrodes. The cyclic voltammograms (CVs) of different modified CPE electrodes were obtained in the potential range of -200 – -600 mV in 0.1M PBS (pH 7.0). No redox peak is observed for the CVs of bare CPE electrode (figure 5(a)) and Mn_2O_3 Nps/ CPE electrode (here not shown). Compared with bare CPE electrode, the background current of Mn_2O_3 Nps-modified CPE electrode is apparently larger, which indicates that the effective electrode surface area is significantly enhanced by use of Mn_2O_3 Nps to modify the surface of CPE electrode. However, the CVs of Cyt_c / Mn_2O_3 Nps / CPE give a pair of well-defined redox peaks at -500 and -475 mV at scan rate of 100 mV/s^{-1} respectively (figure 5(b)), characteristic of heme Fe (III)/Fe (II) redox couples of Cyt_c , suggesting that direct electron transfer has been achieved between Cyt_c and Mn_2O_3 Nps-modified CPE electrode. The difference of anodic and cathodic peak potential values were calculated as $\Delta E = 25$ mV. The redox peaks were attributed to the redox reaction of the Cyt_c electroactive center. The formal potential (E^0) for the Cyt_c redox reaction on the Cyt_c / Mn_2O_3 Nps /GCE was -487.5 versus reference electrode (SCE). The formal potential (E^0) in all electrochemical studies, estimated as the midpoint of reduction and oxidation potentials. The Mn_2O_3 Nps could facilitate fast direct electron transfer between redox proteins and electrode surface. As you know, Cyt_c is the only common heme protein in which the heme is bound to the protein by a covalent linkage. In the Cyt_c three-dimensional structure, the hydrophobic aminoacids cluster about the heme on the inside of the molecule and the hydrophilic residues tend to lie on the surface of the molecule. This protein structure could change oxidative iron state (Fe^{3+}) to reductive state (Fe^{2+}) and vice versa by electron transfer. We used of this electron transfer in designing a new biosensor for H_2O_2 detection.

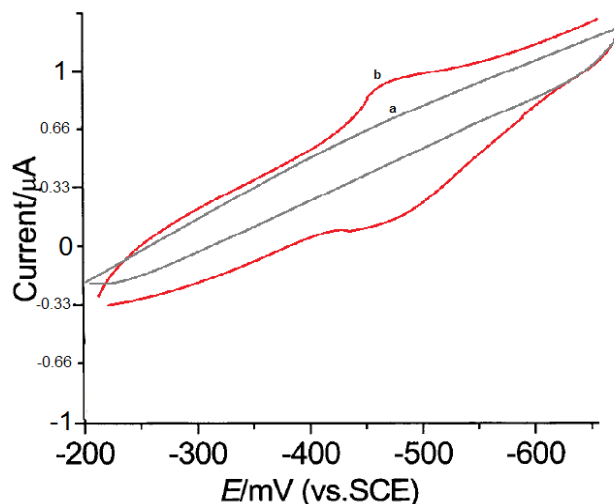
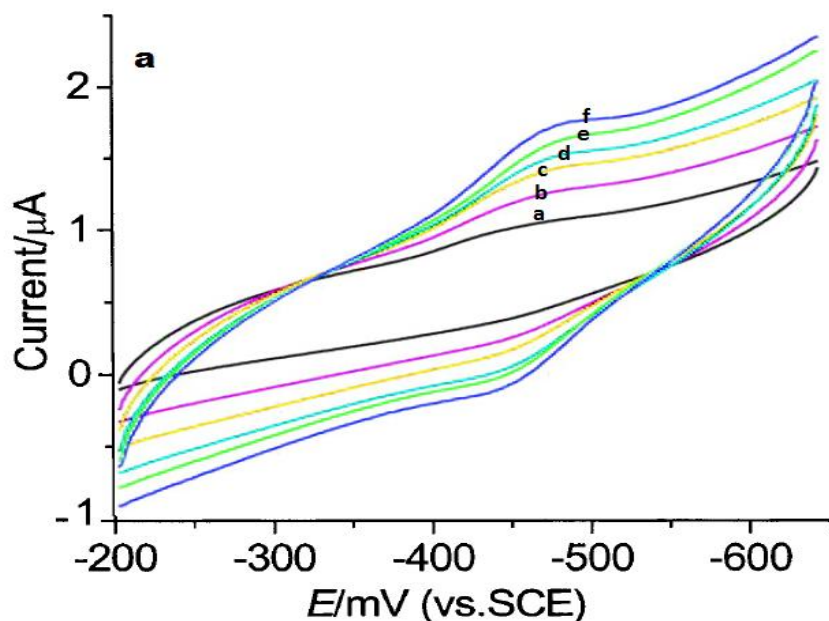


Figure 5. CVs of (a) bare CPE and (b) Cyt c / $\text{Mn}_2\text{O}_3\text{Nps}$ / CPE in 0.1 M phosphate buffer (in 0.1 M PBS and scan rate. 100 mV/s^{-1}).

Fig. 6(a) shows the CVs of the Cyt c / $\text{Mn}_2\text{O}_3\text{Nps}$ / CPE in 0.1 mol L^{-1} phosphate buffer solution (PBS) of pH 7.0 at different scan rates from 50 mVs^{-1} to 500 mVs^{-1} . The peak currents increased and the cathodic and anodic peak potentials exhibited a small shift along with the increase of scan rate. At the same time, the cathodic and anodic peak currents increased linearly with the scan rate (not $v^{1/2}$), as shown in Fig. 6(b); in this picture It can be seen that the redox peak currents increased linearly with the scan rate, the correlation coefficient was 0.9933 ($i_{pc} = 0.0023v + 0.7283$) for cathodic peak and 0.9951 ($i_{pa} = -0.0012v - 0.1373$) for anodic peak respectively. This phenomenon suggested that the redox process was an adsorption-controlled and the immobilized Cyt c was stable.



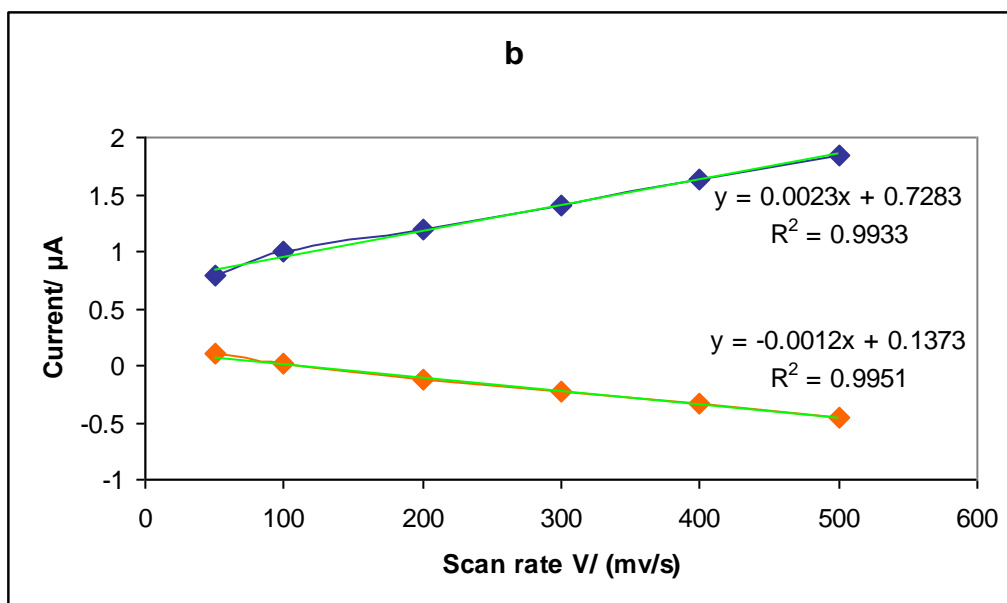


Figure 6. (a) CVs of Cyt c / Mn₂O₃Nps / CPE at various scan rates, from inner to outer; 50(a), 100(b), 200(c), 300(d), 400(e) and 500(f) mV s⁻¹, (b) the relationship between the peak currents (ipa, ipc) vs., the sweep rates; blue lines are reductive peaks and orange lines are oxidative peaks.

All these results indicated that the Cyt_c immobilized on Mn₂O₃Nps / CPE surface controlled and quasi-reversible electrochemical reaction process. When the peak-to-peak separation (ΔE) was larger than 200 mV, the apparent heterogeneous electron transfer rate constants (ks) would be easily calculated with the help of Laviron’s equations [42-43] as follows:

$$E_{p, \text{ cathodic}} = E^0 + \frac{RT}{\alpha F} \ln \frac{RTk_s}{\alpha Fv} \tag{1}$$

$$E_{p, \text{ anodic}} = E^0 + \frac{RT}{(1-\alpha)F} \ln \frac{RTk_s}{(1-\alpha)Fv} \tag{2}$$

$$\Delta E_p = E_{p, \text{ anodic}} - E_{p, \text{ cathodic}} = \frac{RT}{\alpha(1-\alpha)F} \tag{3}$$

$$[\log k_s = \alpha \log(1-\alpha) + (1-\alpha) \log \alpha - \log \frac{RT}{nFv} - \frac{\alpha(1-\alpha)nF\Delta E_p}{2.3 RT}] \tag{4}$$

Where α is the electron transfer coefficient. Here, n is the number of transferred electrons at the rate of determining reaction. The number of electrons transferred in the electrode reaction (n) for a reversible couple can be determined from the separation between peak potentials.

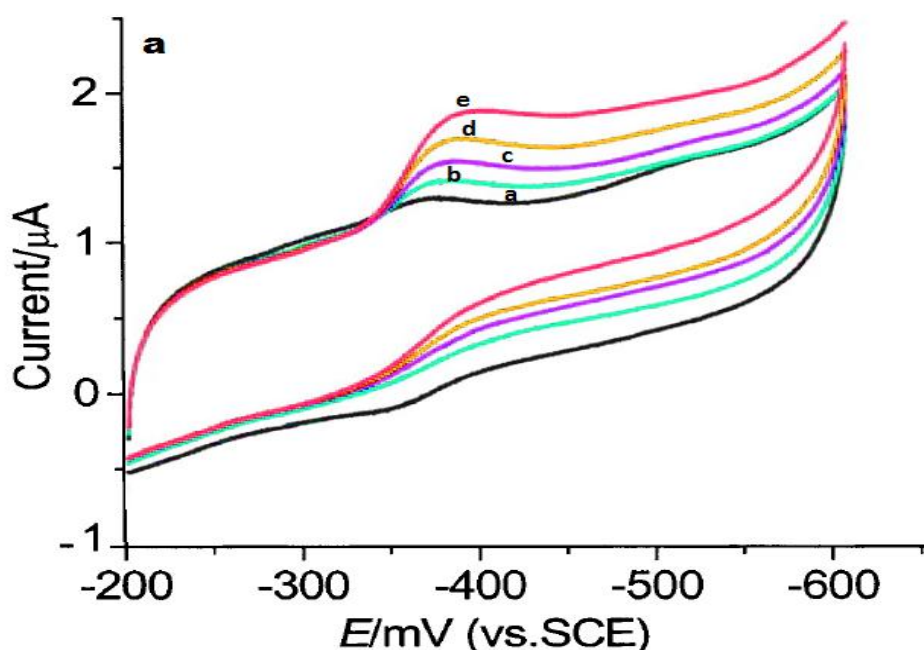
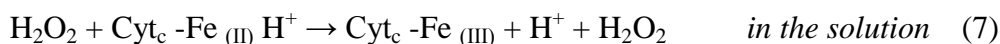
$$\Delta E_p = E_{p, \text{ anodic}} - E_{p, \text{ cathodic}} = \frac{0.059}{n} \tag{5}$$

R, T and F are gas, temperature and Faraday constant, respectively (R = 8.314 J mol⁻¹ K⁻¹, F = 96493 C/mol, T = 298 K) and ks is the apparent heterogeneous electron transfer rate constants which

can be calculated according to ΔE_p versus $\ln v$. The value of k_s was calculated to be 1.7 s^{-1} , which is much higher than that of direct electrochemistry of Cyt c on electrodeposited nickel oxide Nps (0.23 s^{-1}) [44], or direct electron Transfer of cytochrome c on ZnO Nps modified carbon paste electrode (0.64 s^{-1}) [45]. The k_s value directly shows that Cyt c / $\text{Mn}_2\text{O}_3\text{Nps}$ / CPE complex together enhanced the electron transfer rate between Cyt c and $\text{Mn}_2\text{O}_3\text{Nps}$ / CPE.

3.5. Design a H_2O_2 biosensor by use of reduction peaks of Cyt c / $\text{Mn}_2\text{O}_3\text{Nps}$ / CPE

The electrocatalytic reactivity of Cyt c / $\text{Mn}_2\text{O}_3\text{Nps}$ / CPE toward H_2O_2 was investigated by CVs. Fig. 7 (a) displays different CVs obtained for the H_2O_2 biosensor in PBS (pH 6.0) containing varied concentration of H_2O_2 in the absence of oxygen. The catalytic reduction of H_2O_2 at the biosensor can be seen clearly in Fig. 7 (a). With the addition of H_2O_2 , the reduction peak current increases obviously while the oxidation peak current decreases (Fig. 7 (a)), indicating a typical electrocatalytic reduction process of H_2O_2 . However, no similar cathodic peak corresponding to the reduction of H_2O_2 can be observed at bare CPE, $\text{Mn}_2\text{O}_3\text{Nps}$ / CPE electrode under the same condition, so it can be concluded that Cyt_c immobilized on $\text{Mn}_2\text{O}_3\text{Nps}$ / CPE shows good catalytic activity toward H_2O_2 . The decreases of oxidative peak happen together with the increases of the reductive peak of Cyt_c / $\text{Mn}_2\text{O}_3\text{Nps}$ / CPE. This electro-catalytic process could be expressed as follows mechanism (equation 6 and 7):



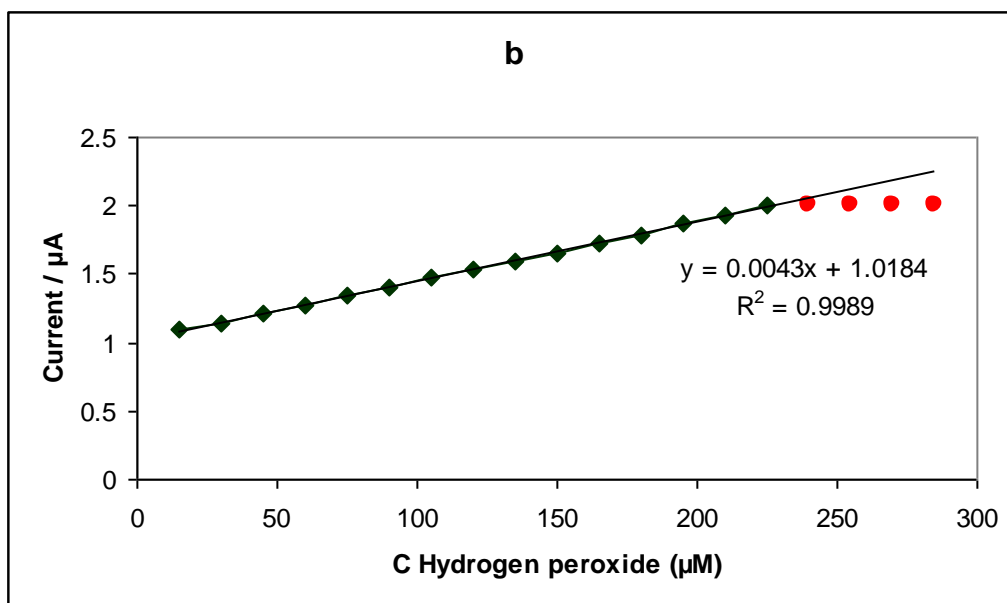


Figure 7. (a) CVs obtained for Cyt_c / Mn₂O₃Nps / CPE in 0.1M phosphate buffer solution (pH 7.0) for different concentrations of H₂O₂ and (b) the relationship between cathodic peak current of Cyt_c and different concentrations of H₂O₂ (scan rate: 100 mVs⁻¹).

The calibration curve (Figure 7b) shows the linear dependence of the cathodic peak current on the H₂O₂ concentration in the range of 15 to 225 μM. In Figure 7(b) at higher concentration of H₂O₂, the cathodic peak current decreased and remains constant. As can be observed, the sensor response shows good linearity in this range. The correlation factor, R^2 was found to be 0.9989. Since the H₂O₂ released is in relatively small micro-molar range, sensor response at such low concentrations assumes great significance. This implies electrocatalytic property of electrode. H₂O₂ detection in micro-molar range is of importance in plant&animal physiology [46-47]. In general, H₂O₂ is released as a stress response to structural damage in plant tissues [48] and also its level involved in a number of biological events and intracellular pathways that have been linked to several diseases [49-50].

4. CONCLUSION

Today nanotechnology provides many easy and cheap ways for us. In this study we used of this novel science in electrochemistry and biology. According to special properties of nanomaterials, when we used of Mn₂O₃ Nps in designing a biosensor, our results improved. Our designed biosensor could detect H₂O₂ in the range of 15 to 225 μM, and detection of this amount is very important in medical and industrial works and diagnostic applications.

References

1. Sun, Y. Metal Nanoplates on Semiconductor Substrates. *Adv. Funct. Mater.*, 20 (2010) 3646.

2. El-Deab, M. S.; Ohsaka, T. *Angew. Chem., Int. Ed.* 45 (2006) 5963.
3. Na, H. B.; Lee, J. H.; An, K.; Park, Y. I.; Park, M.; Lee, I. S.; Nam, D.-H.; Kim, S. T.; Kim, S.-H.; Kim, S.-W.; et al. *Angew. Chem., Int. Ed.* 46 (2007) 5397.
4. Gnanam, S.; Rajendran., V. *J. Sol-Gel Sci. Technol.* 58 (2011) 62.
5. Astruc, D., F. Lu, et al. *Angew. Chem. Int. Ed.* 44 (2005) 7872.
6. Somorjai, G., F. Tao, et al. *Top. Catal.* 47(2008) 14.
7. Zhao J, O'Daly JP, Henkens RW, Stonehuerner J, Crumbliss AL. *Biosens Bioelectron*, 11 (1996) 493.
8. Vo-Dinh T, Cullum BM, Stokes DL. *Sens Actuators*, 74 (2001) 2.
9. Van Gerwen P, Laureyn W, Laureys W, Huyberechts G, Op De Beeck M, Baert K, et al. *Sens Actuators*, 49 (1998) 73.
10. Ramsay, G. Commercial Biosensors; in the series Chemical Analysis; Winefordner, J.D., Ed.; *John Wiley & Sons Inc.: New York*, 1998.
11. Masoud Negahdary, Asadollah Asadi. *Int. J. Electrochem. Sci.*, 7 (2012) 5185.
12. Masoud Negahdary, Seyedeh Anousheh Sadeghi, *Int. J. Electrochem. Sci.*, 7 (2012) 6059.
13. Gholamreza Mohseni , Masoud Negahdary, *Int. J. Electrochem. Sci.*, 7 (2012) 7033.
14. Farough Salimi, Masoud Negahdary, *Int. J. Electrochem. Sci.*, 7 (2012) 7225.
15. Roya Malekzadeh, Masoud Negahdary, *European Journal of Experimental Biology*, 2 (2012) 454.
16. Trasatti, S.; Petrii, O. A. *Pure Appl. Chem.*, 63(1991) 711.
17. K.G.Lim and G.T.R.P almore, *Biosens. Bioelectron.* 22 (2007) 941.
18. M. Fedurco, *Coord. Chem. Rev.* 209 (2000) 263.
19. F.A. Armstrong, A.M. Bond, H.A.O. Hill, B.N. Oliver, I.S.M. Psalti, *J. Am. Chem. Soc.* 111 (1989) 9185.
20. A.E. Kasmi, J.M. Wallace, E.F. Bowden, S.M. Binet, R.J. Linderman, *J. Am. Chem. Soc.* 120 (1998) 225.
21. J. Wei, H. Liu, A.R. Dick, H. Yamamoto, Y. He, D.H. Waldeck, *J. Am. Chem. Soc.* 124 (2002) 9591.
22. R. Swanson, B.L. Trus, N. Mandel, G. Mandel, O.B. Kallai, R.E. Dickerson, *J. Biol. Chem.* 252 (1977) 759.
23. T. Takano, B.L. Trus, N. Mandel, G. Mandel, O.B. Kallai, R. Swanson, R.E. Dickerson, *J. Biol. Chem.* 252 (1977) 776.
24. J. M. Cooper, K. R. Greenough, and C. J. McNeil, *J. Electroanal. Chem.* 347 (1993) 267.
25. K. Tammeveski, T. T. Tenno, *Biol. Med.* 25 (1998) 973.
26. T. M. Cotton, S. G. Schulz, R. P. van Duyne, *J. Am. Chem. Soc.* 102 (1980) 7960.
27. K. Niki, J. R. Sprinkle, and E. Margoliash, *Bioelectrochem.* 55 (2002) 37.
28. M. Collinson, E. F. Bowden, and M. J. Tarlov, *Langmuir* 8 (1992) 1247.
29. G. Chen, J. Zhao, X. Liu, G. Gao, J. Huang, G. Li, *J. Biotechnol.* 127 (2007) 653.
30. Sedigheh Hashemnia, Shima Khayatzadeh, Ali Akbar Moosavi-Movahedi, Hedayatollah Ghourchian, *Int. J. Electrochem. Sci.*, 6 (2011) 581.
31. J. Hong, A. A. Moosavi-Movahedi, *Electrochimica Acta*, 52 (2007) 6261.
32. Masoud Negahdary, Somaye Rad, *Advanced Studies in Biology*, 4(2012) 103.
33. C. Ren, Y. Song, Z. Li, G. Zhu, *Anal. Bioanal. Chem.*, 381 (2005) 1179.
34. Hurdis, E.C.; Hendrik Romeyn, *J. Anal. Chem.* 26 (1954) 320.
35. Matsubara, C.; Kawamoto, N.; Takamura, K. *Analyst*, 117(1992) 1781.
36. Aizawa, M.; Ikariyama, Y.; Kun, H. *Anal. Lett.* 17 (1984) 555.
37. K.Wu, J.Fei, W.Bai, S.Hu, *Anal. Bioanal. Chem.* 376 (2003) 205.
38. Haiming Fan, Lintao Yang, *Nanotechnology.*, 15 (2004) 37.
39. Jeremy Ramsden, *Essentials of Nanotechnology*, Ventus Publishing ApS. 2009.
40. H. Ju, S. Liu, B. Ge, F. Lisdat, F.W. Scheller, *Electroanalysis*, 14 (2002) 141.
41. H. Fan, L. Yang, W. Hua et al., *Nanotechnology*, 15 (2004) 37.

42. E. Laviron, *J. Electroanal. Chem.*, 101 (1979) 19.
43. E. Laviron, *J. Electroanal. Chem.*, 100 (1979) 263.
44. Abdolmajid Bayandori Moghaddam , Mohammad Reza Ganjali, *Journal of Electroanalytical Chemistry.*, 614 (2008) 83.
45. Masoud Negahdary, Saeed Rezaei-Zarchi, *ISRN Biophysics.* 2012(2012) 1.
46. J. D. Willey, R. J. Kieber, *J. Atmos. Chem.* 25 (1996) 149.
47. B. C. Faust and J. M. Allen, *Environ. Sci. Technol.* 27 (1993)1221.
48. W. Dröge, *Physiol. Rev.* 82 (2002) 47.
49. J. Nordberg and E. S. J. Arnér, *Free Radic Biol. Med.* 31 (2001) 1287.
50. T. Finkel and N. J. Holbrook, *Natures London.* 408 (2000) 239.